Proceedings of the International Conference on Oxide Materials for Electronic Engineering, May 29–June 2, 2017, Lviv

ORR Electrocatalysis on Cr^{3+}, Fe^{2+}, Co^{2+}-Doped Manganese(IV) Oxides

G. Sokolsky[a,*], L. Zudina[a], E. Boldyrev[b], O. Miroshnikov[a], N. Gauk[a] and O.Ya. Kiporenko[c]

[a]National University of Food Technologies, Kyiv, Ukraine

[b]Institute of General and Inorganic Chemistry of National Academy of Science of Ukraine, Kyiv, Ukraine

[c]Bogomolets National Medical University, Kyiv, Ukraine

The ionic dopant additives have different mechanisms of their influence upon MnO_2 electrocrystallisation process and depending on dopants added the following polymorphs are stabilised: α-MnO_2 (hollandite, $I4/m$) — NH_4^+; γ-MnO_2 (ramsdellite, $Pbnm$) — Co^{2+}, Fe^{2+}; layered polymorph δ-MnO_2 (birnessite, $C2/m$) — Cr^{3+}. The defect states of intergrowth method in ramsdellite matrix and twinning, OH groups studied by X-ray diffraction and the Fourier transform infrared mtehod, respectively, indicate their high content in case of Fe^{2+} and Co^{2+}-doped manganese dioxide. CVA oxygen reduction reaction peaks were established after experiments in alkaline electrolytes and dioxygen (argon, air) atmosphere. Activity of doped samples studied is comparable with other published data. Both doped with Co^{2+} and Fe^{2+} samples display maximal currents and some distinctive features in oxygen reduction reaction.

DOI: 10.12693/APhysPolA.133.1097

PACS/topics: 61.66.Fn, 61.72.–y, 85.40.Ry

1. Introduction

The word "electrocatalysis" was first used by Grubb [1] in 1963 at the investigations of fuel cells. Electrocatalysis as a phenomenon has the advantages of electrode reaction intensification. The lower overvoltage and the higher current densities at the same electrode potential the more prospective is electrode material considered for various applications including oxygen reduction (ORR) and oxygen evolution (OER) reactions [2].

Manganese(IV) oxides demonstrate diversity of structure behaviour. The variety of polymorphs and strong dependence of properties on origin of the samples or preparation methods have been established [3, 4]. Tunnelled structures of β-MnO_2 (pyrolusite), γ-MnO_2 (ramsdellite), α-MnO_2 (hollandite) have different size of structure channels formed by MnO_6 octahedrons with the ending member of this structure family that is layered δ-MnO_2. Some of them are able to defects of intergrowth. For instance, γ-MnO_2 products represent randomly distributed intergrowth microdomains of pyrolusite (0.23 nm $\times$0.23 nm tunnel structure), which are made of [MnO_6] units with either edge or corner sharing (De Wolff defects) [5, 6].

MnO_2 is obtained more frequently by anode electrodeposition of Mn(II) species known as electrochemical manganese dioxide (EMD). The foreign ions being added in an electrolyte make the scope of electrodeposition method broader. As shown earlier, these ions influence upon polymorphic composition, structure, size, and morphology of crystallites of the electrodeposition product [7–9]. We have already developed electrolytic doping procedure [10–12] that makes possible the direct preparation of nonstoichiometric transition metal oxide-based thin film cathodes for lithium rechargeable batteries by electrodeposition [13]. The thin film chromium oxide based cathode plating electrodeposited in the presence of lithium ions becomes rechargeable at the lithium content in the film of about 0.02wt%. Electrolytic doping by Li-ions is shown to improve discharge characteristics of solid state MnO_2 electroreduction process in alkaline medium. We have observed correlation between the concentration of lithium and copper additive in an electrolyte and capacity of electroreduction process in 9 M KOH [14]. There is a good potential of Fe-doped MnO_2 as an electrocatalyst of phenol oxidation [7].

The Suib research group studied chemically obtained manganese dioxide (CMD) functionality improvement via its doping by foreign ions [15]. The new evidence of ion induced promotion of activity enhancement of inverse micelle templated mesoporous manganese oxides for aerobic oxidation reactions has been revealed in [16]. Ion promoted mesoporous manganese oxides (UCT-18-X, X= Mg^{2+}, Ca^{2+}, K^+, Na^+ and Cs^+) having trace amount of alkali metal ions were tested for selective aerobic alcohol oxidation and the catalytic activity following the order of UCT-1 <UCT-18-Mg <UCT-18-Ca <UCT- 18-K<UCT-18-Na <UCT-18-Cs. Nanosized α-MnO_2 with Sn-doping is shown to be the electrode material with improved capacity retention for Li ion batteries recently [17].

Oxide compounds of manganese were known as one of the most effective oxygen electrocatalysts alternative to noble metals for many decades [18]. Manganese oxides are used in commercial primary zinc-air batteries [19–21].

*corresponding author

However, their ORR activity is limited by the low electrical conductivity of the oxides, which can be improved by adding carbon blacks or hybridizing with conductive agents like carbon nanotubes or graphenes [22–24] or introducing oxygen vacancies [25]. MnO_2 α-polymorph with nanowire morphology demonstrated the exceptional 3000 mA h g^{-1} capacity for promising Li-air battery (LAB) technology only recently [26]. The crystal structure of this polymorph consists of 2×2 tunnels formed by edge- and corner-sharing MnO_6 octahedrons with the ability to accommodate both Li^+ and O^{2-} or O_2^{2-} in case of aqueous or nonaqueous types of LAB. As shown in [27, 28], the redox pairs of Mn(III)/Mn(IV), the Jahn–Teller distorted Mn(III) ions of surface layer of the crystal lattice are the most probable active sites of oxygen reduction and oxygen oxidation reactions (ORR (OER)). In addition, Mn_2O_3 prominent activity as an air electrode was established [28]. Therefore, not only manganese oxides with hollandite structure should be studied.

Manganese oxides have no appreciable OER activity and should be combined with another OER electrocatalyst in LAB. Co and Fe-based materials have been shown to be excellent OER catalysts and are stable in alkaline solutions [29–31].

The proper combination of the ORR and OER electrocatalysts is crucial for the electrochemical performance. MnO_x and Co–Fe were sequentially electrodeposited on carbon paper to fabricate bifunctional catalysts MnO_x/Co–Fe for zinc-air batteries in [32]. The electrochemical properties of the hybrid MnO_x/Co–Fe catalysts demonstrated higher ORR and OER activity compared with MnO_x and Co–Fe alone. A Zn–air battery using MnO_x/Co–Fe catalysts exhibited good discharge-recharge performance and a cycling efficiency of 59.6% that is comparable with Pt/C catalysts. Electrodeposited MnO_x/Co–Fe showed strong adhesion to gas diffusion layer and was stable for 40 h of battery cycling.

The phase composition and structure defects have profound influence on manganese(IV) oxides materials activity. Therefore, the purpose of this work was to study influence of induced by dopant ions (Cr^{3+}, Fe^{2+}, Co^{2+}) changes in phase composition, defect states on the ability of manganese(IV) oxides to be oxygen electrocatalyst of ORR.

2. Experimental

As shown earlier [33], composition and properties of manganese oxide compounds obtained from fluoride-containing electrolytes can be easily controlled. They can be produced at high rates since fluoride-containing complexes in electrolytes of manganese(II) have high mobility at electrodeposition of manganese dioxide [12]. Manganese(IV) oxide samples were electrodeposited galvanostatically (i = 10 A/dm^2) at the platinum plate anode and the vitreous carbon plate as an auxiliary electrode. The pristine fluorine-containing electrolyte consisted of 0.1 M HF + 0.7 M $MnSO_4$ and the dopant additives in the electrolyte were sulfates of the following concentration: 1.5 M NH_4^+ (sample 2), 0.01 M Cr^{3+} (sample 3), 0.01 M Fe^{2+} (sample 4), 0.01 M Co^{2+} (sample 5) [1]. The dopants concentrations were chosen taking into account solubility of these compounds, their electrochemical behaviour, i.e. the ability to be incorporated into the electrodeposit in minor amounts, and also the preliminary experimental results. The precipitates of doped electrolytically manganese dioxide were formed at the bottom of electrolytic bath due to the high current density applied. They were separated by decantation and filtration after electrodeposition experiment, rinsed with distilled water till the negative reaction on $BaCl_2$, dried 3 h at 100–110 °C to eliminate physically sorbed water.

The serial sample of chemical manganese dioxide (CMD, Pridneprovsk Chemical Plant, Kamianske, Ukraine) was taken for the sake of comparison (sample 1). Samples used, their numbers and some properties are indicated in Table I.

TABLE I

Composition and some structure parameters of standard (1) and doped (2–5) manganese dioxide samples obtained by anode electrodeposition at the presence of ionic additives.

Samples	1	2	3	4	5
origin/dopant	CMD*	NH_4^+	Cr^{3+}	Fe^{2+}	Co^{2+}
dopant ion concentration in electrolyte [mol/l]	–	1.5	0.01	0.01	0.01
Mn(total) [mass%]	61.9	59.7	55.2	44.2	45.2
dopant ion content in samples [mass%]	–	–	3.9	0.26	0.012
phase components	γ	$\alpha+\gamma$	$\delta+\gamma$	$\gamma+\beta$	γ
Tw [%]	22.6	25.9	–	46.9	65.0
P_r	0.36	0	–	0.11	0.22

*Sample of chemical manganese dioxide produced at Pridneprovsk Chemical Plant (Kamianske, Ukraine)

Chemical composition of samples was determined by atomic absorption spectroscopy (AAS) as a total content of manganese and dopant-ion in mass%. The Fourier transmission infrared (FTIR) spectra were taken on a FSM-1201 Fourier spectrometer using standard KBr pellet methods. X-ray diffraction (XRD) of the products was registered on a DRON-3 X-ray diffractometer with Cu K_α radiation (λ = 0.154184 nm) or Mo K_α(λ = 0.070930 nm). The multiphase composition and grain size of the samples were investigated by Powder Cell for Windows v. 2.3 computer program. The defects are usually responsible for activity and they were analysed in ramsdellite-containing samples in accordance with the Chabre–Pannetier model [34] and in case of CuK_α radiation as follows (2.1)–(2.5):

$$Tw\ [\%] = 100 - 68.17\Delta 2\theta, \tag{2.1}$$

$$\delta(Tw) = -0.0054Tw - 8.9 \times 10^{-5}Tw^2,$$

$$(Tw < 55\%), \tag{2.2}$$

$$\delta(Tw) = -0.56 \quad (Tw \geq 55\%), \tag{2.3}$$

$$\delta(DW) = 2\theta(110) - \delta(Tw) - 21.808(2\theta\ [^\circ]), \tag{2.4}$$

$$P_r = 0.602\delta(DW) - 0.198\delta^2(DW) + 0.026\delta^3(DW), \tag{2.5}$$

where Tw [%] is a twinning, $\Delta 2\theta$ is a distance between (221) and (240) reflexes, δTw is the shift of line 110 corrected for microtwinning [deg 2θ], P_r is a γ/β-intergrowth fraction or De Wolff defects ($0 \leq P_r \leq 1$).

Electrochemical experiment was carried out with a computer-controlled potentiostat–galvanostat (IPC-PRO, STC "Volta", Russia) at room temperature. Cyclic voltammetry (CVA) and linear sweep voltammetry (LSV) measurements were performed at 0.001–0.3 V/s potential scan rates and electrode potential window of (–1.1)–(+1.6) V. Electrode potentials were registered and shown vs. Ag/AgCl, KCl(saturated) reference electrode. The electrolyte containing 0.3 M LiOH was saturated with oxygen (argon) 30 min before each experiment.

Carbon paste electrode (CPE) was assembled to study manganese dioxide samples electrocatalytic activity in ORR. CPE was a thoroughly grounded mixture of doped manganese dioxide: graphite in 70:30 ratio and polytetrafluoroethylene (PTFE) emulsion ($S = 0.045$ cm^2) placed into silicone tube with metallic collector inside supplied with the Luggin capillary. Three electrode cell contained also glass–carbon plate auxiliary electrode and silver/silver chloride reference electrode.

3. Results and discussion

Chemical composition of the samples studied is shown in Table I. The content of dopant-additive in samples is low excepting Cr^{3+} content of which exceeds several percents. Manganese content is lower than its theoretical value for MnO_2 in Table I due to nonstoichiometric nature of electrodeposition product including cationic vacancies, γ/β-intergrowth, Mn^{3+}-, and other defects [6, 35, 36]. The influence of transition metal (TM) ion dopants is an additional factor of nonstoichiometry in MnO_2. Their ability to parasitic redox transitions (samples 3–5) causes the significant drop of the manganese dioxide current yield. The mechanism of incorporation and localization of dopant additives in electrocrystallisation products have been actively studied [37, 38].

The following main phase components were isolated by XRD technique depending on dopants added: α-MnO_2 (hollandite, $I4/m$) — NH_4^+; γ-MnO_2 (ramsdellite, $Pbnm$) — Co^{2+}, Fe^{2+}; layered polymorph δ-MnO_2 (birnessite, $C2/m$) — Cr^{3+} (Table I, Fig. 1). The most intensive peaks of distinctive phase components in samples 3–5 are shown in Fig. 1. Samples 4, 5 display different types of disorder in ramsdellite structure and low crystallinity. The main peak of ramsdellite structure at $2\theta = 22^\circ$ is the most intensive and broadened in Co-doped sample 5 unlike Fe-doped sample 4 in addition to the weak peak of individual phase component of β-MnO_2 (instead of γ/β−intergrowth) in the latter sample (Fig. 1). The most intensive reflex around $2\theta = 38^\circ$ is common for

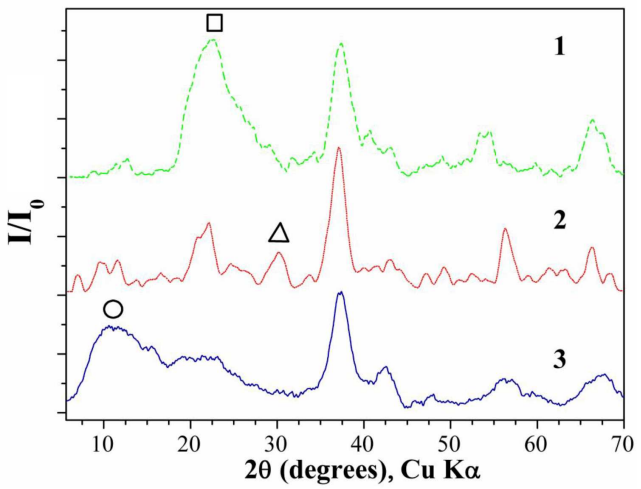

Fig. 1. XRD-patterns of doped samples 5 (curve 1), 4 (2), 3 (3). Symbols indicate phase component (□ — ramsdellite as a main phase component, Δ — pyrolusite, ○ — birnessite).

tunnel manganese dioxide polymorphs [7, 34]. Some additional details of structure interpretation were published elsewhere [7].

This structure phase analysis is in agreement with thermodynamics of hollandite phase since foreign ions like NH_4^+ in structure channels decrease its free energy significantly [39] as a result of influence of entropic factor. Co^{2+}, Fe^{2+} are able to manganese substitution in oxide framework, whereas Cr^{3+} causes the pillaring effect stabilising MnO_x layers in birnessite structure [15].

Pyrolusite/ramsdellite microdomains intergrowth (P_r) and twinning defects in ramsdellite-containing samples (Tw) calculated by Eqs. (2.1)–(2.5) [34] are demonstrated in Table I. M^{2+}-doped samples reveal high concentration of twinning. Probably, these ions are responsible for cationic vacancies in MnO_6 octahedrons and heterovalent substitution of manganese by dopant M^{3+}-ion making twinning more energetically favourable state in oxide framework. Thus, Fe^{2+} displays the strong reducing activity toward manganese dioxide framework, but cobalt has higher standard electrode potential Co^{3+}/Co^{2+} and probably could be immobilized in crystal structure of manganese dioxide by the "Co immobilization-manganese oxide dissolution reaction" mechanism proposed for manganese oxide minerals by Manceau et al. [40]. It includes low pH Mn^{3+} disproportionation at the first stage:

$$2Mn^{3+}(\text{surf.}) \leftrightarrows Mn^{4+}(\text{surf.}) + \square + Mn^{2+}(\text{solution}),$$

$$Co^{2+}(\text{solution}) + \square_1 + Mn^{3+}(\text{surf.}) \leftrightarrows Co^{2+}(\text{surf.}) + Mn^{3+}(\text{surf.}),$$

$$Co^{3+}(\text{surf.}) + Mn^{2+}(\text{surf.}) \leftrightarrows Co^{3+}(\text{surf.}) + \square_2 + Mn^{2+}(\text{solution}),$$

where □ are the cationic vacancies filled with Co^{2+} ($\square_1$) and new ones created by aqueous Mn^{2+} formed ($\square_2$).

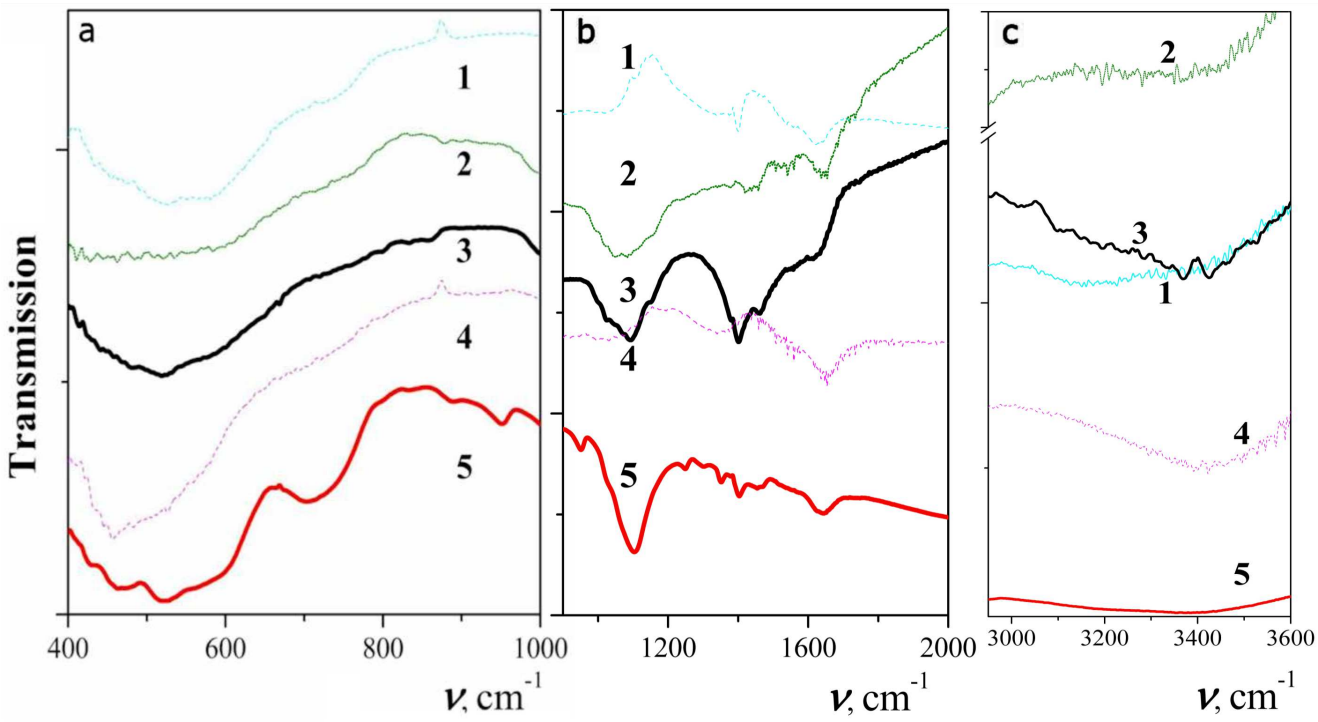

Fig. 2. FTIR spectra of investigated samples 0.01 M Fe^{2+} (spectrum 1), 0.01 M Cr^{3+} (spectrum 2), serial CMD (spectrum 3), 0.01 M Co^{2+} (spectrum 4), 1.5 M NH_4^+ (spectrum 5) in the range from 400 to 1200 cm^{-1} (a), from 1000 to 2000 cm^{-1} (b), from 3000 to 3600 cm^{-1} (c).

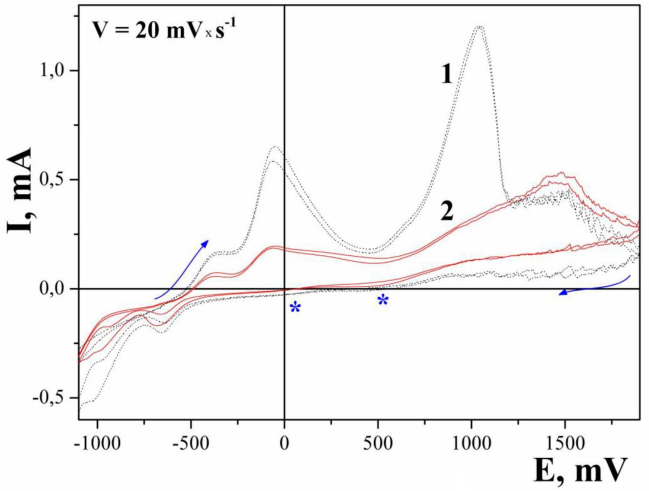

Fig. 3. CVA of CPE with Fe^{2+}-(1) and Co^{2+}-(2) doped γ-MnO_2 samples 4, 5 in O_2 saturated 0.3 M LiOH (V = 20 mV s^{-1}, stars indicate ORR).

The significant broadening of ramsdellite polymorph peak (110) at $2\theta = 22°$ in Co-doped manganese dioxide comparing with other ramsdellite containing EMDs could be the indirect confirmations of Co^{2+} incorporation into manganese oxide framework (Fig. 1). It is worth noting that CoOOH (heterogenite, *Pbnm*; PDF-2 card #26-0480, $a = 0.4353$, $b = 0.9402$, $c = 0.2840$ nm) is isostructural to MnOOH (PDF-2 card #24-0713, $a = 0.4560$, $b = 0.1070$, $c = 0.2870$ nm), and ramsdellite MnO_2 polymorph (PDF-2 card #82-2169, $a = 0.9322$, $b = 0.445$, $c = 0.2848$ nm). Goethite, α-FeO(OH), also exhibits an orthorhombic symmetry (*Pnma*) with unit cell parameters $a = 0.995$, $b = 0.301$, $c = 0.462$ nm unlike CrOOH [41]. The existence of solid solutions of manganese and cobalt of oxide-hydroxide nature was additionally confirmed by our further XRD analysis of data for heavy doped by cobalt samples of manganese dioxide published in [42].

It should be pointed out that both additives decrease γ/β-intergrowth fraction in doped samples (P_r parameter or De Wolff defects, Table I) calculated by Eq. (2.5). Samples have nanorod shape of crystallites with diameter of about 10–20 nm as shown by transmision electron microscopy (TEM) previously [12].

Infrared spectroscopy of manganese oxides is sensitive to amorphous component in addition to phase components with long-range order [43] unlike XRD. Our FTIR spectra were registered in the range of 400–4000 cm^{-1} (Fig. 2). The similarity of behaviour of the samples in the FTIR spectra region of 400–1000 cm^{-1} can be seen, where the main bands are attributed to the stretching mode of the MnO_6 octahedrons (Fig. 2a). The stretching mode of MnO_6 octahedrons along the double-chain is located at 708 cm^{-1} in the FTIR spectra of sample 2 with hollandite structure [44]. Sample 2 has relatively sharp

peaks indicative of a well-developed hollandite-type α-MnO_2 structure with an interstitial space consisting of narrow one-dimensional (2×2) channels. Infrared bands at about 430, 470, 520, 550, 600 cm^{-1} in the same spectrum are in agreement with [43]. Spectra of samples 3–5 are diffuse and have similarity to sample 1 with ramsdellite structure in this region due to complex composition and nonstoichiometry of electrodeposition products in agreement with XRD data (Table I and [7]).

The vibration modes at about 1100, 1420, 1650 cm^{-1}, and 3150, 3400 cm^{-1} were assigned to the bending and stretching modes of water and/or OH groups, respectively (Fig. 2b–c). Doped by Co^{2+} and Fe^{2+} EMD samples 4–5 (Fig. 2b, spectra 1,4) have all bending mode bands in the 1000–2000 cm^{-1} region but of very diffuse nature due to low crystallinity. Sample 4 doped by Fe^{2+} has well-defined stretching mode at 3150 cm^{-1} (Fig. 2c, curve 1).

CVAs of doped MnO_2 CPE in 0.30 M LiOH solution saturated with oxygen are demonstrated in Fig. 3 at $V = 20$ mV s^{-1}. Peaks of ORR become visible in mA range of currents in our CVA experiments after electrolyte saturation with oxygen or prolonged anode polarisation at potentials higher than 1 V (vs. Ag/AgCl) at oxygen evolution (OER, Fig. 3). The weak two steps of ORR are usually detectable at low rates of potential scan (below 75 mV s^{-1}) since oxygen reduction kinetics is very slow. They can be seen in the range of potentials –0.2 and 0.7 V (stars indicate ORR steps in Fig. 3) and are the charge transfer controlled with the Tafel slopes b that are in agreement with 60 and 120 mV of ORR detected on Pt electrode correspondingly [2]. OER peaks are observed at the reverse direction of CVA scan after about 1.0 V. Potential oscillations on CVA are good indicators of OER due to insulating properties of evolved oxygen bubbles.

Analysis of ORR activity of investigated samples is shown in Table II. Fe^{2+}, and Co^{2+} doped samples display similar behaviour with two weak peaks of ORR currents. The FTIR spectra similarity of these materials, first of all bending vibrations of OH-groups and water, probably causes the same influence of dopant-ion on the active sites of surface in ORR. The high content of Tw reflects, in turn, cationic vacancies and heterovalent substitution of manganese in sites of oxide framework of samples 4, 5. It indicates the possibility of influence of the mobile Ruetschi protons and OH-groups of positions with heterovalent substitution on ORR (OER) activity [36]. These samples have two well-defined $2e^-$ steps of ORR with maximal current unlike samples 1–3. ΔE (E_{OER} $-E_{ORR}$) is close to 1.0 V which is in agreement with published data [45]. Chromium additive stabilising birnessite polymorph causes negative influence on ORR electrocatalytic activity.

The anode current of OER makes up 56 mA/cm^2 for sample 2 which is evaluated as the diffusion-limiting current and it is by about 40 times larger than ORR currents on this sample. These results are in agreement with data published elsewhere [45]. The highest activity of α-MnO_2 nanorods among other MnO_2 polymorphs in ORR (OER) was demonstrated in [26]. In our opinion it can be attributed to availability of structure tunnels to small O_2 and H_2O molecules. The broadened nature of ORR (OER) peaks on α-MnO_2 unlike Fe-doped γ-MnO_2 sample are in agreement with the latter hypothesis and Ref. [26]. The high activity of Fe^{2+}-doped MnO_2 indicates the positive role of Fe^{3+}/Fe^{2+} redox pairs as active sitĺs of surface states.

TABLE II

ORR electrochemical parameters of samples 1–5 ($V = 0.02$ V/s).

Sample	1 CMD	2 NH_4^+	3 Cr^{3+}	4 Fe^{2+}	5 Co^{2+}
ORR E_1 [V]	0.591	-	-	0.547	0.544
I_1 [mA/cm^2]	1.36	-	-	1.18	1.38
ORR E_2 [V]	-	-0.028	-0.111	0.023	-0.015
I_2 [mA/cm^2]	-	1.24	0.56	0.29	0.33

MnO_2 CPE 1 exhibits also two reduction peaks (at about –0.6 V and –1.05 V) and two oxidation peaks (at about –0.35 V and –0.1 V) which were ascribed to manganese dioxide redox behaviour. Graphite electrode has by the order of magnitude lower currents of the same processes.

4. Conclusions

The electrolytic doping procedure expands practical application of electrochemical manganese dioxide due to the control of chemical and phase compositions. The ionic dopant additives of NH_4^+, Cr^{3+}, Fe^{2+}, Co^{2+} have different mechanisms of their influence upon electrocrystallization process. Among them incorporation of cobalt into manganese oxide framework, template effects of alkali metal ions [8] and NH_4^+, "pillaring" action of Cr^{3+} were proposed on the basis of our and published elsewhere data. It is shown that depending on dopants added different polymorphs are stabilised: α-MnO_2 (hollandite, $I4/m$) — NH_4^+; γ-MnO_2 (ramsdellite, $Pbnm$) — Co^{2+}, Fe^{2+}; layered polymorph δ-MnO_2 (birnessite, $C2/m$) — Cr^{3+}. Defect states of intergrowth in ramsdellite matrix and twinning, OH groups studied by XRD and FTIR, respectively, indicate their high content in case of Fe^{2+} and Co^{2+}-doped manganese dioxide.

The effects of oxygen/ electrocatalysis in alkaline medium saturated by oxygen were discussed for doped electrolytically manganese dioxide. CVA ORR peaks were established after experiments in dioxygen (argon, air). It is confirmed that activity of all doped samples is comparable with other published data. Both doped with Co^{2+} and Fe^{2+} samples display maximal currents and some distinctive features in ORR. It is proposed that combination of Co^{2+} and Fe^{2+} additives could be prospective for LAB cathode application.

References

[1] J.O'M. Bockris, Z.S. Minevski, *Electrochim. Acta* **39**, 1471 (1994).

[2] C. Song, J. Zhang, in: *PEM Fuel Cell Electrocatalysts and Catalyst Layers: Fundamentals and Applications*, Ed. J. Zhang, Springer, London 2008, p. 89.

[3] A.F. Wells, *Structural Inorganic Chemistry*, Oxford University Press, Oxford 1984

[4] *Handbook of Manganese Dioxide Battery Grade*, Eds. D. Glover, B. Schumm, A. Kozawa, International Battery Material Association (IBA Incorporated), 1989.

[5] J.E. Post, *Proc. Natl. Acad. Sci. USA* **96**, 3447 (1999).

[6] P.M. de Wollf, *Acta Crystallogr.* **12**, 341 (1959).

[7] G.V. Sokol'skii, S.V. Ivanov, N.D. Ivanova, E.I. Boldyrev, T.F. Lobunets, *J. Water Chem. Technol.* **34** 227 (2012).

[8] G.V. Sokolsky, S.V. Ivanov, E.I. Boldyrev, N.D. Ivanova, T.F. Lobunets, *Solid State Phenom.* **230**, 85 (2015).

[9] G. Sokolsky, N. Ivanova, S. Ivanov, Ye. Boldyrev, in: *NANOSMAT 2007, Alvor, Algarve (Portugal)*, 2007, Abstracts book, p. 168.

[10] F. Fabregat-Santiago, E.M. Barea, J. Bisquert, G.K. Mor, K. Shankar, C.A. Grimes, *J. Am. Chem. Soc.* **130**, 9 (2008).

[11] G. Sokolsky, S. Ivanov, N. Ivanova, Ye. Boldyrev, M. Kakazey, *Materials Today*, Virtual Conference on Nanotechnology (2012.

[12] G.V. Sokolsky, S.V. Ivanov, N.D. Ivanova, Ye.I. Boldurev, O.V. Kobulinskaya, M.V. Demchenko,*Acta Phys. Pol. A* **117**, 86 (2010).

[13] E.I. Boldyrev, N.D. Ivanova, G.V. Ivanov, O.A. Stadnik, *J. Solid State Electrochem.* **17**, 2213 (2013).

[14] G. Sokolsky, N. Ivanova, S. Ivanov, Ye. Boldyrev, in: *5th Spring Annual Meeting of the ISE, Dublin (Ireland)*, International Society of Electrochemistry, Lausanne 2007, p. 227.

[15] S.L. Suib, *Acc. Chem. Res.* **41**, 479 (2008).

[16] S. Biswas, A.S. Poyraz, Y. Meng, C.-H. Kuo, C. Guild, H. Tripp, S.L. Suib, *Appl. Catal. B Environm. Appl. Catal. B Environm.* **165**, 731 (2015).

[17] A.M. Hashem, A.M. Abdel-Latif, H.M. Abuzeid, H.M. Abbas, H. Ehrenberg, R.S. Farag, C.M. Julien, *J. Alloys Comp.* **509**, 9669 (2011).

[18] K. Matsuki, H. Kamada, *Electrochim. Acta* **31**, 13 (1986).

[19] A. Sumboja, X.M. Ge, F.W.T. Goh, B. Li, D.S. Geng, T.S.A. Hor, Y. Zong, Z.L. Liu, *ChemPlusChem* **80**, 1341 (2015).

[20] S. Lee, G. Nam, J. Sun, J.S. Lee, H.W. Lee, W. Chen, J. Cho, Y. Cui, *Angew. Chem.-Int. Ed.* **55**, 8599 (2016).

[21] T. Reddy, *Handbook of Batteries* McGraw-Hill, 2011.

[22] K.B. Liew, W.R.W. Daud, M. Ghasemi, K.S. Loh, M. Ismail, S.S. Lim, J.X. Leong, *Int. J. Hydrogen En.* **40**, 11625 (2015).

[23] K.H. Wu, Q.C. Zeng, B.S. Zhang, X. Leng, D.S. Su, I.R. Gentle, D.W. Wang, *Chemsuschem* **8**, 3331 (2015).

[24] P.-C. Li, C.-C. Hu, T.-H. You, P.-Y. Chen, *Carbon* **111**, 813 (2017).

[25] F. Cheng, T. Zhang, Y. Zhang, J. Du, X. Han, J. Chen, *Angew. Chem. Int. Ed.* **52**, 2474 (2013).

[26] A. Débart, A.J. Paterson, J. Bao, P.G. Bruce, *Angew. Chem.* **120**, 4597 (2008).

[27] A.S. Ryabova, F.S. Napolskiy, T. Poux, S.Ya. Istomin, A. Bonnefont, D.M. Antipin, A.Y. Baranchikov, E.E. Levin, A.M. Abakumov, K. Gwénaëlle, E.V. Antipov, G.A. Tsirlina, E.R. Savinova, *Electrochim. Acta* **187**, 161 (2016).

[28] A.S. Ryabova, A. Bonnefont, P. Zagrebin, T. Poux, R.P. Sena, J. Hadermann, A.M. Abakumov, G. Kéranguéven, S.Y. Istomin, E.V. Antipov, G.A. Tsirlina, E.R. Savinova, *CHEMELECTROCHEM* **3**, 1667 (2016).

[29] S. Luo, D.B. Zhou, *J. Electrochem. Soc.* **161**, A23 (2013).

[30] L. Jörissen, *J. Power Sourc.* **155**, 23 (2006).

[31] M.S. Burke, M.G. Kast, L. Trotochaud, A.M. Smith, S.W. Boettcher, *J. Am. Chem. Soc.* **137**, 3638 (2015).

[32] Ming Xiong, D.G. Ivey, *J. Electrochem. Soc.* **164**, A1012 (2017).

[33] N.D. Ivanova, E.I. Boldyrev, K.N. Pimenova, G.V. Sokol'skii, I.S. Makeeva, *Russ. J. Appl. Chem.***71**, 1269 (1998).

[34] Y. Chabre, J. Pannetier, *Prog. Solid State Chem.* **23**, 1 (1995).

[35] J. Brenet, *J. Power Sourc.* **4**, 183 (1979).

[36] P. Ruetschi, R. Giovanioli, *J. Electrochem. Soc.* **135**, 2663 (1988).

[37] O. Shmychkova, T. Luk'yanenko, R. Amadelli, A. Velichenko, *J. Electroanal. Chem.* **774**, 88 (2016).

[38] N.D. Sakhnenko, M.V. Ved', D.S. Androshchuk, S.A. Korniy, *Surf. Eng. Appl. Electrochem.***52**, 145 (2016).

[39] S. Fritsch, E.J. Post, S.L. Suib, A. Navrotsky, *Chem. Mater.***10**, 474 (1998).

[40] A. Manceau, V.A. Drits, E. Silvester, C. Bartoli, B. Lanson, *Am. Mineral.* **82**, 11 (1997).

[41] M. Mohapatra, S. Anand, *Int. J. Eng. Sci. Technol.* **2**, 127 (2010).

[42] G. Sokolsky, N. Ivanova, S. Ivanov, T. Tomila, Ye. Boldyrev, *Sci. Sintering* **39**, 273 (2007).

[43] T. Barudžija, N. Cvjetićanin, D. Bajuk-Bogdanović, M. Mojović, M. Mitrić, *J. Alloys Comp.* **728**, 259 (2017).

[44] C.M. Julien, M. Massot, C. Poinsignon, *Spectrochim. Acta Part A Mol. Biomol. Spectrosc.* **60**, 689 (2004).

[45] Chung-Hao Kuo, I.M. Mosa, S. Thanneeru, V. Sharma, Lichun Zhang, S. Biswas, M. Aindow, S. Pamir Alpay, J.F. Rusling, S.L. Suib, Jie He, *Chem. Commun.* **51**, 5951 (2015).